Atmospheric Research 176–177 (2016) 1–9

Contents lists available at ScienceDirect

Atmospheric Research

journal homepage: www.elsevier.com/locate/atmosres

Aerosol radiative forcing efficiency in the UV-B region over central Argentina

Gustavo G. Palancar [a], Luis E. Olcese [a], Bethania L. Lanzaco [a], Mariana Achad [a], María Laura López [b], Beatriz M. Toselli [a,*]

[a] Departamento de Físico Química/INFIQC/CLCM/CONICET, Facultad de Ciencias Químicas, Universidad Nacional de Córdoba, Ciudad Universitaria, Córdoba 5000, Argentina
[b] Facultad de Matemática, Astronomía y Física/IFEG/CONICET, Universidad Nacional de Córdoba, Ciudad Universitaria, Córdoba 5000, Argentina

ARTICLE INFO

Article history:
Received 14 September 2015
Received in revised form 16 February 2016
Accepted 17 February 2016
Available online 24 February 2016

Keywords:
UV-B radiation
Aerosols
AERONET
MODIS
Radiative forcing

ABSTRACT

AEROSOL Robotic Network (AERONET), Moderate Resolution Imaging Spectroradiometer (MODIS) and global UV-B (280–315 nm) irradiance measurements and calculations were combined to investigate the effects of aerosol loading on the ultraviolet B radiation (UV-B) reaching the surface under cloudless conditions in Córdoba, Argentina. The aerosol radiative forcing (ARF) and the aerosol forcing efficiency (ARFE) were calculated for an extended period of time (2000–2013) at a ground-based monitoring site affected by different types and loading of aerosols. The ARFE was evaluated by using the aerosol optical depth (AOD) at 340 nm retrieved by AERONET at the Cordoba CETT site. The individual and combined effects of the single scattering albedo (SSA) and the solar zenith angle (SZA) on the ARFE were also analyzed. In addition, and for comparison purposes, the MODIS AOD at 550 nm was used as input in a machine learning method to better characterize the aerosol load at 340 nm and evaluate the ARFE retrieved from AOD satellite measurements. The ARFE at the surface calculated using AOD data from AERONET ranged from (−0.11 ± 0.01) to (−1.76 ± 0.20) Wm^{-2} with an average of −0.61 Wm^{-2}; however, when using AOD data from MODIS (TERRA/AQUA satellites), it ranged from (−0.22 ± 0.03) to (−0.65 ± 0.07) Wm^{-2} with an average value of −0.43 Wm^{-2}. At the same SZA and SSA, the maximum difference between ground and satellite-based was 0.22 Wm^{-2}.

1. Introduction

Aerosols are emitted to the atmosphere by natural and anthropogenic processes and are important from the point of view of air quality and radiative transfer. Aerosols influence the Earth energy budget directly by scattering and absorbing the incoming solar radiation and indirectly by changing the microphysical and, hence, the radiative properties, amount, and lifetime of clouds (IPCC, 2007, and references therein).

Due to their complex effects on atmospheric processes, aerosols are one of the atmospheric constituents with the largest uncertainty regarding their contribution to the radiative forcing (IPCC, 2007). Because of the variability in sources and sinks, different aerosol components are associated with different geographical areas, and the residence time in the troposphere is relatively short (Haywood and Boucher, 2000). Thus, in contrast to greenhouse gases, aerosol loading and optical properties exhibit large spatial and temporal variability.

The amount of ultraviolet (UV) radiation reaching the surface of the Earth is of extreme importance as its variations have a direct impact on living organisms and atmospheric chemistry (McKenzie et al., 1991). Under cloudless skies, ozone and aerosols are the main atmospheric constituents that influence the transfer of UV radiation in the atmosphere. One way to obtain information about the optical properties of aerosols is by performing radiation measurements at the surface or at different platforms such as satellites (Yu et al., 2006). Ground-based observations are measurements at a single point and therefore cannot account for spatial variation unless a large network is operational. Satellite observations provide spatial coverage but usually only at specific times. Hence, the interaction and the constant comparison between them are important tools to understand the forcing of aerosols at a local and global scale.

The importance of the harmful effects of solar UV radiation has warranted a significant effort to understand all aspects of the UV radiative transfer in the atmosphere. One of the aspects to be improved is the knowledge of the role played by the atmospheric aerosols, and thus special attention must be paid to absorbing aerosols such as particles from biomass burning and mineral dust. Nevertheless, the influence of aerosols on UV radiation still shows considerable uncertainties, which can become potential error sources, especially in UV products from satellite measurements or in global climate models. For instance, under cloud-free conditions, the accuracy of satellite UV estimations is limited mainly by the knowledge of highly variable aerosol properties.

Despite the importance of aerosols in modifying the radiation budget in the Earth-atmosphere system, there are still large uncertainties in the aerosol radiative forcing (ARF) on a local and regional scale

* Corresponding author. Tel.: +54 351 5353866; fax: +54 351 4334188.
E-mail address: tosellib@fcq.unc.edu.ar (B.M. Toselli).

http://dx.doi.org/10.1016/j.atmosres.2016.02.016
0169-8095/

(Papadimas et al., 2012). ARF at any layer in the atmosphere is defined as the difference in the net fluxes (down minus up) with and without aerosols at that layer (Bush and Valero, 2003). Depending on the nature of aerosols and the surface albedo, the ARF may yield negative or positive values. The former corresponds to a cooling effect while the latter indicates a warming effect (Chen et al., 2015). The magnitude and sign of ARF is determined by the different aerosol species, their size distribution, and their chemical and optical characteristics (Ramachandran et al., 2012). There are a number of studies on radiative forcing of aerosols in the UV region of the solar spectrum. For example, García et al. (2006) estimated the aerosol radiative forcing efficiency (ARFE) in the interval 290–325 nm, reporting values of -0.16 Wm^{-2} at Canadian Observatories, representatives of background conditions, and -0.36 Wm^{-2} at 340 nm at Ispra, Italy, a site representative of urban and industrial aerosols. At Thessaloniki, Greece, Kazadzis et al. (2009) informed an ARFE value in the wavelength range of 325–340 nm of -0.71 Wm^{-2} (AOD at 340 nm); these measurements are for the period 1998–2006. Direct radiative forcing measurements of Saharan dust in the Mediterranean (Lampedusa Island) have been performed by Meloni et al. (2004) reporting ARFE values in the UV-B range from -0.40 to -0.57 Wm^{-2}. Nikitidou et al. (2013) informed ARFE values between -0.35 and -0.069 Wm^{-2} depending on SZA in the UV-B region; these measurements were carried out at Uccle, Belgium and represent a West European site.

In the present study, we assessed, for the first time at central Argentina, the ARF and the ARFE (i.e., the ARF per unit of aerosol optical depth, AOD) under cloudless conditions in the UV-B region (280–315 nm) by using AOD at 340 nm retrieved from ground-based measurements from the AERONET and by the MODIS instrument (Terra and Aqua satellites), previously validated against AERONET. To do that, we took advantage of our long-term data set (2000–2013) of global UV-B irradiance measurements. Theoretical UV-B irradiance values under aerosol-free conditions were obtained by running the tropospheric ultraviolet and visible radiation model (TUV) (Madronich, 1987).

Thus, as an outcome of this work, we present new results that will contribute to quantify and reduce the uncertainties in the influence of aerosols on climate. Quantifying and reducing these uncertainties are critical to understand climate change over the industrial period and to improve predictions of future climate change for different emission scenarios, especially in the Southern Hemisphere, where studies are much less frequent.

2. Data and methodology

2.1. UV-B solar irradiance measurements

Irradiance measurements were carried out using a pyranometer YES (Yankee Environmental System, Inc.) model UV-B1, which measures global UV-B irradiance (280–315 nm). The pyranometer was factory calibrated, and its spectral response function is given elsewhere (Palancar and Toselli, 2002, 2004). The uncertainties in the irradiance measurements are mainly related to the instrument geometry and materials used to build it. Uncertainties are intrinsic to the instrument measurement system (temperature control, transmittance and sensitivity of the different filters, cosine response, spectral response, etc.), which lead to a maximum of 5% difference between two identical calibrated instruments as described in the work of Dichter et al., 1993. More details about uncertainties, calibration, and maintenance of the pyranometer can be found in López et al. (2012). Observations were recorded as half a minute average values in the period 2000–2013. Cloudless conditions were periodically assured by direct observers. Because visible and infrared wavelengths are more sensitive to cloud presence, the daily course of total irradiance (300–3000 nm), measured with a YES model TSP-700 pyranometer, was used to double check the cloudless condition at all times. The instruments were mounted on a wide-open area in the University Campus in Córdoba City, Argentina (31.24ºS, 64.11ºW, 470 m.a.s.l.), located southwest of downtown. The radiometers were placed on a cement yard surrounded by low buildings, trees, grass, paved streets and bare soil.

2.2. UV-B irradiance modeling

The TUV radiation model version 4.1 was used for all UV-B model calculations (Madronich, 1987). A sensitivity analysis was carried out using this model in order to establish the best values for the most important parameters in the calculations for Córdoba City (Palancar, 2003). The final setup used in the model was as follows: the wavelength grid was built with 1 nm intervals between 280 and 315 nm; the surface albedo was assumed to be Lambertian, wavelength independent, and with a constant value of 0.05 throughout the year; the extraterrestrial irradiance values were taken from Van Hoosier et al. (1987) and Neckel and Labs (1984). An 8-stream discrete ordinate method and clear sky conditions were used. Total ozone column values were obtained daily by the Total Ozone Mapping Spectrometer (TOMS) instrument onboard Earth Probe spacecraft until 2005 and by the Ozone Monitoring Instrument (OMI) onboard Aura spacecraft since 2006. Due to the low levels of tropospheric UV-B absorbing pollutants like O_3, SO_2, and NO_2 in Córdoba City (Olcese and Toselli, 2002), they were not considered in the model calculations.

2.3. AOD from AERONET

In this study, one of the sources used to obtain the optical properties of the aerosols was a nearby AERONET site, located 28 km from the measurement site. The CIMEL Sun photometer was installed in 1999 at Córdoba CETT (Centro Espacial Teófilo Tabanera), at 31º 30′ S, 64º 24′ W, and was operative until the end of the year 2010. This instrument belongs to AERONET, a federated international network, coordinated by the NASA Goddard Space Flight Center, which currently maintains more than 400 automatic sun/sky radiometers worldwide. Since 1999, the aerosol optical parameters retrieved from AERONET measurements at Córdoba CETT site have allowed to directly consider the characteristic of local aerosols in model calculations. An accuracy assessment of the AERONET retrievals can be found in the work of Dubovik et al. (2000).

AOD_λ (Level 2.0) is calculated as the integral of the atmospheric extinction coefficient from the surface to the top of the atmosphere at a given wavelength. As AOD_λ is measured by direct sun photometry; therefore, it requires accurate ground-based solar spectral radiance measurements (Holben et al., 1998). The wavelength dependence of the AOD is related to the aerosol type and their physical and chemical characteristics. The single scattering albedo (SSA) is a variable correlated with the radiative forcing of the Earth's atmosphere. It is defined as the amount of scattering in relation to the total extinction at a small volume of aerosols. This variable can take values between 0 (a purely absorbing particle) and 1 (a purely scattering particle) and can have important effects on the radiative balance.

2.4. AOD from MODIS

The MODIS instruments were launched aboard the Terra and Aqua satellites in the years 2000 and 2002, respectively, to make global observations of the Earth in a wide wavelength range (Kaufman et al., 1997). In this work, the Atmosphere level 2, collection 5.1, product MOD04_L2 for Terra, and MYD04_L2 for Aqua, were used. All data available for each satellite up to the year 2013 were included. The shortest wavelength retrieved by MODIS is 470 nm, being AOD at 550 nm the generally used product. To obtain an AOD from MODIS in the UV region, a procedure was implemented. Recently, we have presented a method to improve the AOD retrieval from MODIS at 550 nm (Lanzaco et al., 2015). The method is based on machine learning techniques (Artificial Neural Networks, ANN, and Support Vector Machines, SVM), which significantly improve the results of the direct correlation (AOD_{MODIS} against $AOD_{AERONET}$). Machine learning is a subfield of artificial intelligence which develops algorithms that can empirically learn from the behavior

or the properties of a given data set. In these methods, a training data set is provided separated into "inputs" and "outputs," and the algorithm tries to find a connection between them. The outputs are the variables to be predicted, while the inputs are the variables which will feed the algorithm (Vapnik, 1995). A portion of the data set was not used during the training; it was reserved only for validation purposes. In this work, both ANN and SVM methods were used to obtain an improved AOD at 340 nm using AOD at 550 nm and meteorological data as inputs.

The model was trained for Cordoba CETT station, seeking to improve the MODIS AOD_{340} retrievals and to provide a simple and reliable way to correct local bias and outliers. The AOD retrieved by MODIS at 550 nm ($AOD_{MODIS,\ 550}$) and ground-based meteorological data available within 40 km from the AERONET site were used as inputs. $AOD_{MODIS,\ 550}$ was retrieved for both ocean and land with the best quality data. This data set is available from the Atmosphere Archive and Distribution System (LAADS) website (http://ladsweb.nascom.nasa.gov) and is delivered in Hierarchical Data Format (HDF), with a pixel resolution of 10 km × 10 km (at nadir). To ensure a proper comparison between MODIS and AERONET retrievals, it was necessary to employ a spatiotemporal approach (Petrenko et al., 2012). In this work, the geographical and temporal averages were calculated using the spatiotemporal approach available at MAPSS webpage (http://giovanni.gsfc.nasa.gov/mapss/) for the Córdoba CETT AERONET station (Remer et al., 2008). The output of the models was the AOD_{MODIS} at 340 nm ($AOD_{MODIS,\ 340}$), which was compared to $AOD_{AERONET}$ at the same wavelength ($AOD_{AERONET,\ 340}$), considered as the ground truth data.

2.5. Aerosol radiative forcing

The ARF represents the difference between the instantaneous irradiance measured in a situation with aerosol present and one with aerosol-free condition. The ARF was calculated in the 280–315 nm wavelength range based on the broad band radiometer measurements and on model calculations with the TUV radiative transfer model.

The irradiances calculated by the TUV model showed a very good agreement with the irradiance measurements under aerosol-free conditions. Modeled aerosol-free irradiances were then subtracted from the irradiances in the presence of aerosols for each day from the period (see Eq. (1)) (Bush and Valero, 2003). The advantage of this method is that it can be used to estimate ARF for all type of aerosols, including the background aerosols. The uncertainty in the ARF using this approach was estimated to be around 10% including the uncertainties in modeled and measured radiation fluxes.

The ARF was calculated as

$$ARF = (I_{measured} - I_{modeled}). \quad (1)$$

where $I_{measured}$ is the integral of the radiometer measurements in the 280–315 nm wavelength range at a given SZA value when the aerosols are present, and $I_{modeled}$ is the integral of the corresponding modeled irradiances for the same ozone and SZA, under aerosol-free conditions. The ARFE is the forcing performed per unit of AOD. Using the ARFE, the forcing no longer depends on the aerosol load but on the aerosol type and its characteristics. The ARFE is given by the slope of the linear regression between the ARF and AOD values:

$$ARFE = ARF/AOD_{340}. \quad (2)$$

3. Results and discussion

3.1. UV-B radiation

For the measurement period, the maximum irradiance measured value was 2.50 Wm^{-2} with an average value of 0.89 Wm^{-2}. Overall, 2790 irradiance measurements were used under cloudless conditions, which represent 58% of the whole data set. Fig. 1 shows the daily course of the measured irradiance for several days under different meteorological conditions. Fig. 1a and b show 2 days where the good agreement between UV-B irradiance measurements and TUV model calculations under aerosol-free conditions, can be observed. This result was previously quantified by Palancar and Toselli (2004). They found that the agreement between measurement and model calculation under aerosol-free condition was better than 5% for SZA less than 50º and 10% for SZA between 50º and 70º. Therefore, under cloudless sky conditions, the important reductions in measured UV-B radiation compared to calculated irradiance under aerosol-free conditions can be attributed to the effect of the aerosol loading. In polluted regions, tropospheric aerosols can significantly reduce UV levels (Zerefos, 1997) for several days and under different types of atmospheric conditions. This effect is shown in Fig. 1c for September 19, 2001, in Córdoba City. In a daily average, UV-B radiation on that day was more than 33% lower than in a day with no aerosol present; this was one of the largest reductions of the year due to aerosol loading (the maximum reduction was 44% at 10 a.m.). However, similar systematic aerosol effects are observed every year during the August–November period (Fig. 1c–e). The attenuation of UV-B radiation is often observed in late winter and spring due to the effect of the meteorology of Córdoba City (Palancar and Toselli, 2002). In August and September, strong winds blow during most of the day. Levels of relative humidity are low and a considerable amount of particulate matter is present during most of the month. As a consequence of the wind strength and the lack of rain, particulate matter from natural and anthropogenic origin is not removed from the atmosphere, and it results in the systematic reduction of UV B levels observed during every winter spring period (López et al., 2012; Achad et al., 2013). In every case, the cloudless and aerosol-loaded condition was assured by direct observations. Fig. 2 shows the location of the city in central Argentina together with the wind rose for the region.

3.2. Radiative effects of aerosols using AOD retrieved from AERONET

Several restrictions had to be applied before carrying out the ARFE calculations. First of all, both measurements (irradiance and AOD) had to be as close as possible in time frequency. In this work, UV-B radiation measurements were taken every 30 s. Therefore, there was at most a difference of 29 s between the times in which AERONET provided AOD data and the UV-B irradiance measurement. In this way, we ensure that both measurements were made under the same conditions. Then, the other restriction to evaluate the effects of aerosols was to rule out all the factors that could influence UV-B radiation, such as clouds, snow, ozone, pollutants, albedo, and SZA. In Córdoba City, snow is exceptional, and no data with this phenomenon are present in our measurements. The occurrence of clouds was checked by observing the total global radiation because this range of wavelength is much more sensitive to their presence. Only days with clouds completely absent were used for the calculation. The surface albedo is very low in the UV-B region (0.05) if no snow is present and is almost wavelength independent.

Fig. 3 shows several panels where ARF is plotted at different 5° SZA intervals as a function of $AOD_{AERONET,340}$. To build these plots, four conditions were considered. First, for each point, the difference between the measurement and the calculation had to be larger than 5%. That condition assured that this difference was due to the aerosol effects and not to the model or measurement uncertainties. Second, the AOD had to be larger than 0.1. This was because small AOD are usually affected by larger uncertainties (Dubovik et al., 2000). Third, at least 8 points were required to calculate a linear regression. Finally, the quality of a fit, given by the determination coefficient (R^2), which had to be higher than 0.5 with a p-value smaller than 0.02 for a 95% confidence level to be accepted.

The scatter observed in this figure was associated with variations of other optical properties besides AOD. To determine and understand how these optical properties determine ARF, the slopes of the straight

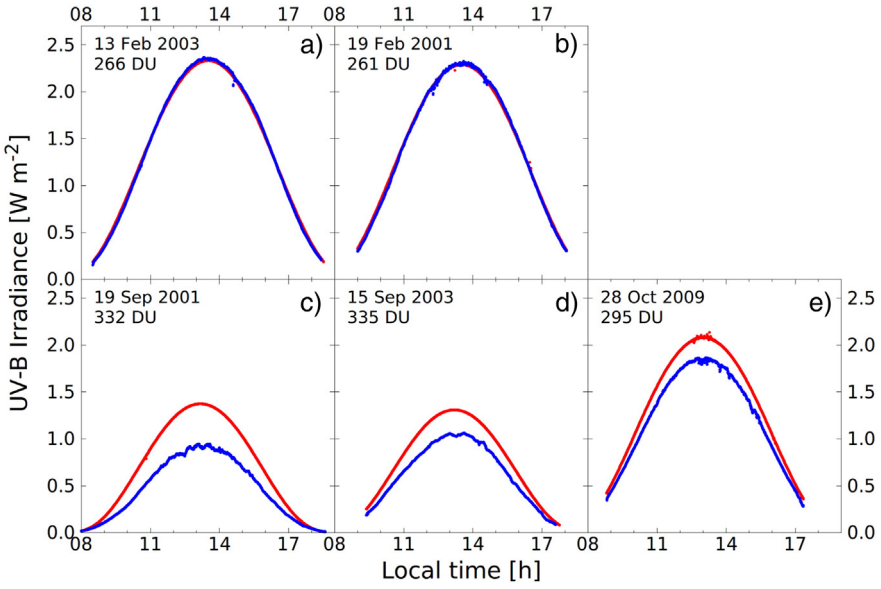

Fig. 1. Daily course of measured (blue line) and modeled (red line) UV-B irradiance in Córdoba City (a and b) for aerosol-free days and (c–e) for days in the presence of aerosols.

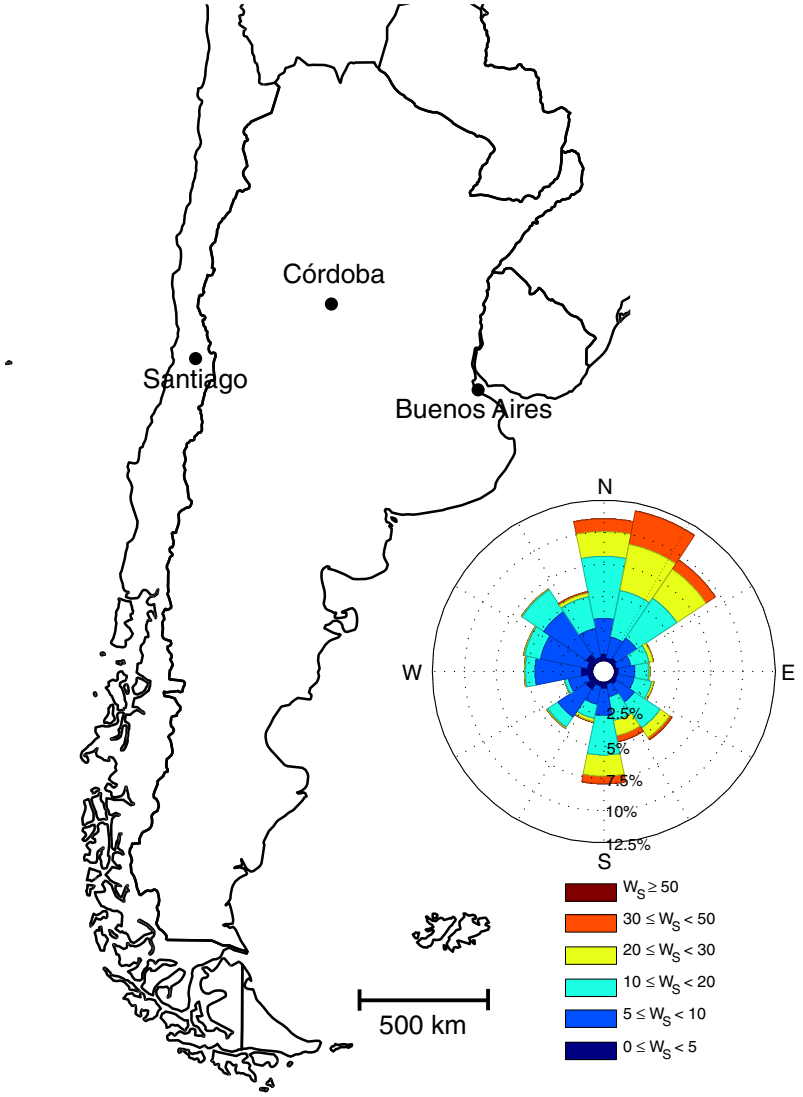

Fig. 2. Map of Argentina, indicating the location of Córdoba City. The inset corresponds to the wind rose for Córdoba city for the 2000–2013 measurement period. WS represents wind speed in m s^{-1}. In the map the cities of Buenos Aires (Argentina) and Santiago (Chile) are also marked for reference purposes.

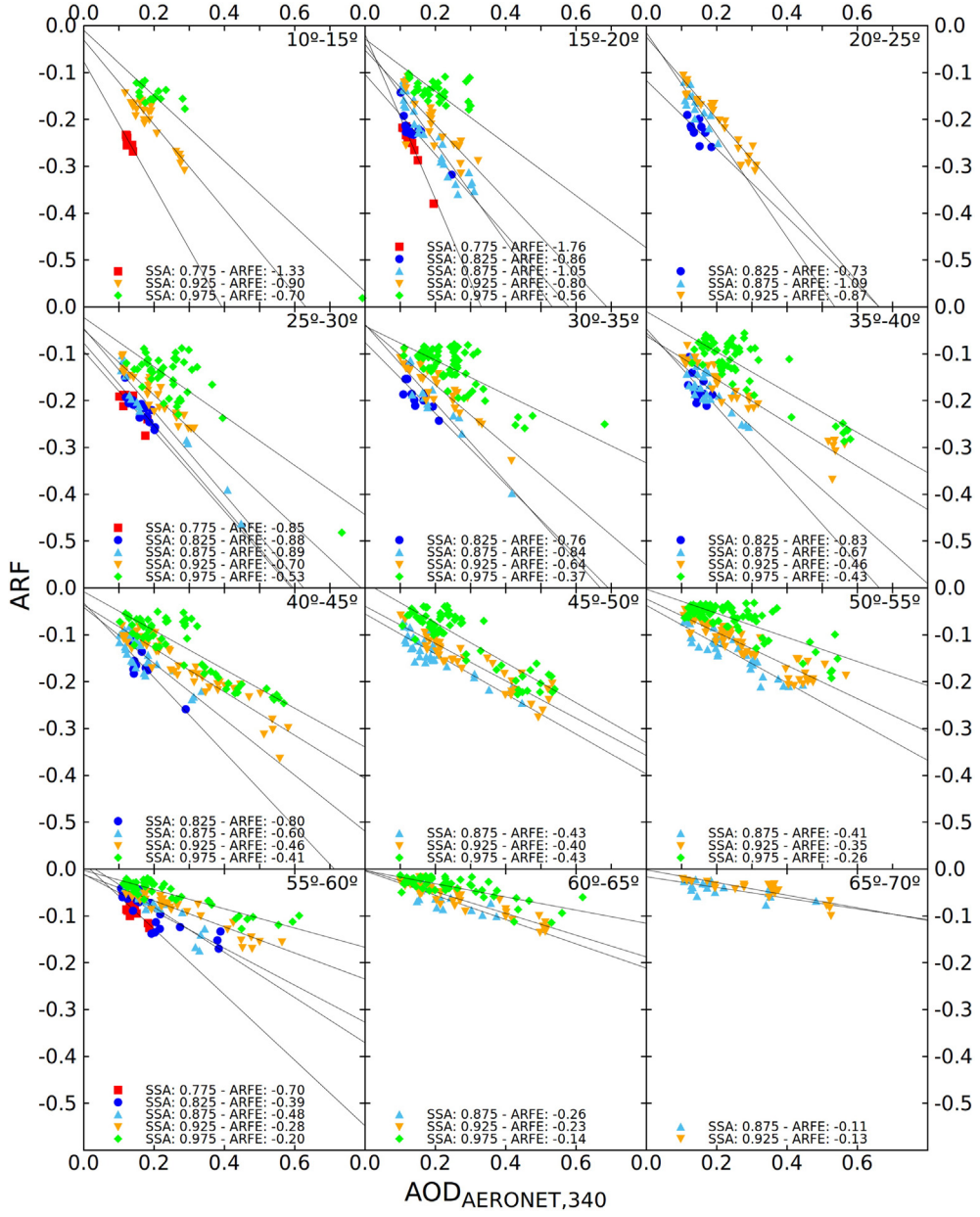

Fig. 3. ARF in the UV-B region as a function of AOD at 340 nm (taken from AERONET). The ARFE for different SZA (5º intervals) and SSA (0.05 unit intervals) are indicated in each panel.

line were evaluated according to the SSA value (i.e., in a small range of 0.05 units) and at different SZA. This procedure was followed because the site is affected by a mixture of at least two types of aerosols (urban and mineral), which are present throughout the year in different combinations (Achad et al., 2013). Therefore, to fit the results to a straight line, the effect for that particular combination needed to be considered. Thus, at every SZA interval, the results were separated according to the SSA value. In order to estimate the aerosol effective SSA, another set of theoretical calculations was performed incorporating the aerosol optical properties taken from the AERONET database (AOD and asymmetry parameter ($g = 0.66$)) in the TUV model. Andrada et al. (2008) showed that this g value is the best one in the UV-B range for local aerosols. As the SSA at 340 nm is not provided by AERONET, we estimated the best SSA value by varying this parameter between 0.6 and 0.99 and taking the value, which made the difference between the irradiance measurements and the TUV calculation closer to zero and less than 5%. As observed in Fig. 3, for the same AOD and SZA range, the SSA modulated and determined the magnitude of ARFE. The calculated ARFE ranged from (-0.11 ± 0.01) up to (-1.76 ± 0.20) Wm^{-2} with an average value of –0.61 and no particular distribution along this range. Ideally, the ordinates in these plots should be equal to zero, which indicates that in the absence of aerosols the radiative forcing should be null. In our plots, ordinates are very close to zero with an average value of –0.03 and always less than –0.1, independently of the SZA and the SSA. These values validate not only the linear adjustments but also the agreement between the clear sky model results and the measurements in the absence of aerosols.

Another way to present the results was by plotting the ARFE values as a function of the SSA (y-axis) and the SZA (x-axis). In this way, the single and combined effects of both variables became clear. This result is presented in Fig. 4. As rain is almost absent from April to October in central Argentina, we calculated ARFE for the dry (April–October) and rainy seasons (November–March) separately. The rainy data set has a large number of data because rain occurs during summer time, when the daily variation of the SZA is larger. Beyond this fact, the difference between the results for these two periods was not significant. Even though throughout the year there are contributions of at least two

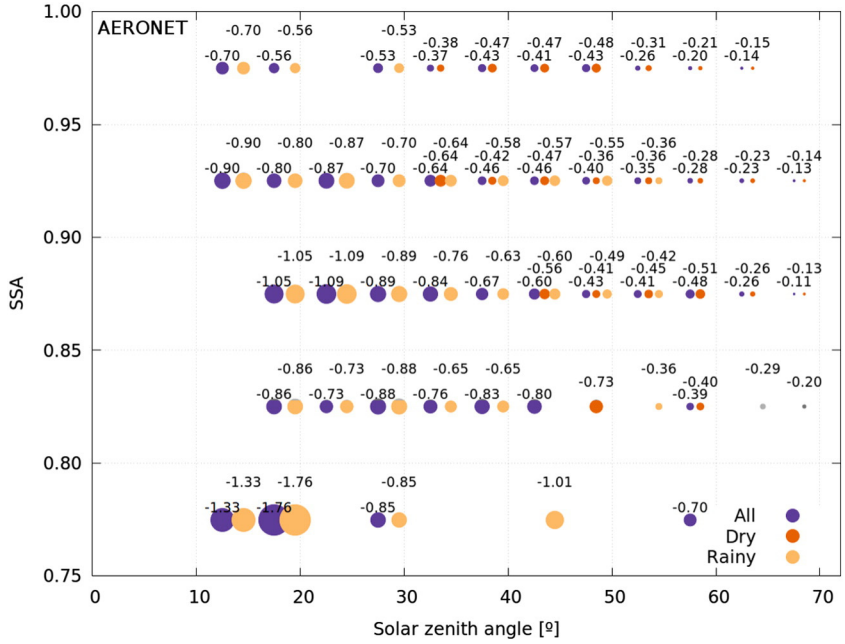

Fig. 4. ARFE in the UV-B region for different SSA and SZA intervals for dry and rainy seasons. AOD values were taken from AERONET. ARFE values correspond to the slopes shown in Fig. 3. Each set of data (all, dry, and rainy) is plotted at the center of the SSA and SZA intervals.

types of aerosols (urban and mineral), the differences in their contributions are not large enough to reflect substantial changes in the ARFE values.

As mentioned above, Fig. 4 clearly shows the effect of SZA on ARFE values. The maximum radiative effect that occurred at the SZA interval of 15°–20° corresponds to a forcing of –1.76 Wm^{-2}. As the SZA increases, the ARFE tends to decrease (absolute value). This is because at solar noon (smallest SZA) the largest absolute differences between the experimental and calculated irradiances are obtained, as observed in Fig. 1. This resulted in larger slopes, and therefore larger ARFE. Moreover, as in the UV region, the diffuse component of the radiation is larger than the direct component at large SZA, the effects of the aerosols are of less importance. A similar trend of ARFE has been observed by Antón et al. (2011) at Granada, Spain, and by Nikitidou et al. (2013) at a typical West European site (Uccle, Belgium). In addition to SZA, ARFE is also affected by changes in the SSA, which reflects the changes in the composition of the particles that determines the relative weight of scattering and absorption on extinction. At the same SZA, ARFE increases in absolute value as SSA decreases (see Figs. 3 and 4). For instance, at SZA interval of 15°–20°, ARFE changes from –1.76 Wm^{-2} at SSA 0.775 down to –0.56 Wm^{-2} at SSA 0.975. As expected, this dependence shows that the stronger aerosol absorption leads to a larger radiative forcing efficiency at surface.

3.3. Radiative effects of aerosol using AOD retrieved from MODIS

Fig. 5 shows the monthly averaged climatology of the ground-based (AERONET) and satellite-derived AOD at 340 nm, for the region around Córdoba City calculated over the period 2000–2010 (MODIS-Terra) and 2002–2010 (MODIS-Aqua). In this plot, only simultaneous AERONET-MODIS measurements were considered. Terra and Aqua data correspond to the improved AOD values according to the methodology presented in Section 2.4 (i.e., $AOD_{MODIS,\ 340}$). For MODIS instrument aboard Terra satellite, the learning machine method that produced the best results was SVM. The linear adjustment between $AOD_{MODIS,\ 340}$ and $AOD_{AERONET,\ 340}$ had a R^2 of 0.79, a root mean square value

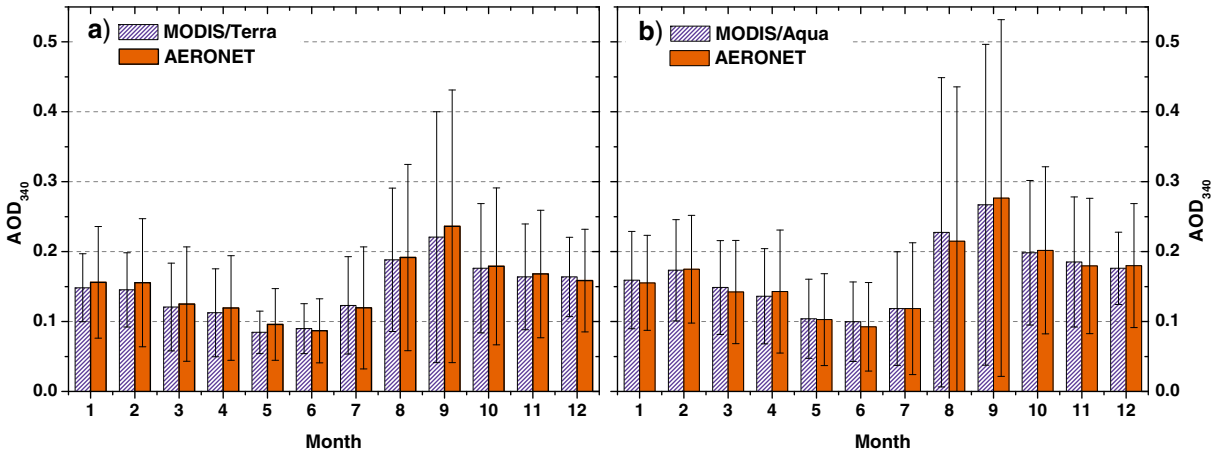

Fig. 5. Monthly averaged AOD at 340 nm retrieved from AERONET and from MODIS for periods 2000–2010 (Terra) and 2002–2010 (Aqua). Only AERONET-MODIS simultaneous measurements were included.

(RMS) = 0.04 and a slope of 0.89. The meteorological variables incorporated as inputs into the model were temperature and relative humidity. For MODIS instrument aboard Aqua satellite, the best model was trained using ANN. In this case, the linear adjustment had a $R^2 = 0.86$, RMS = 0.03, and a slope = 0.87. Only the temperature needed to be incorporated as input, in addition to AOD at 550 nm. As observed from the statistical indicators, both sets of data were in very good agreement. Although Fig. 5 shows that the agreement with AERONET is very good, there are still small differences which can be related to several issues. For example, the differences between the AOD retrievals from Terra and Aqua are expected since these satellites have morning and afternoon overpass times, respectively, and the aerosol load in Córdoba exhibits variations throughout the day. On the other hand, the differences between MODIS-Terra and MODIS-Aqua data could be at least partially explained by the well-known degradation of the optic sensor on Terra (Levy et al., 2013; Cordero et al., 2014). The AOD maximum and minimum, as well as the characteristic variation throughout the year, have its origin in the Córdoba meteorology, as explained in Section 3.1.

Fig. 6 shows the ARF as a function of $AOD_{MODIS,\ 340}$ for several SZA intervals. The straight lines of the fits were performed as explained in Section 3.2, varying also the SSA. The ARFE in this case ranged from (-0.22 ± 0.02) up to (-0.65 ± 0.07) Wm^{-2} with an average value of –0.43. As in the AERONET case, the distribution of the ARFE values did not show any tendency. The ordinates were also very close to zero with a maximum deviation of –0.05 and an average of around –0.02. As in Fig. 4, Fig. 7 shows the effect of the SSA and SZA on ARFE but, in this case, for the satellite retrieved data set.

As shown in this figure, $AOD_{MODIS,\ 340}$ values are less abundant compared to $AOD_{AERONET}$ and are absent below SZA less than 30º. This is mainly because of two facts. First, the Terra and Aqua satellites pass only once a day over our site when the SZA is not at its minimum (Terra in the morning, Aqua in the afternoon). Second, the presence of clouds during summer time (when the minimum SZA occurs) is much more frequent. Consequently, the ARFE calculated with this set of data is not necessarily the same as that presented in Section 3.2. Although the interval of variation of the ARFE values was smaller than in the AERONET case, the average values were not markedly different. This shows that the extreme values observed by AERONET were only sporadic.

3.4. Comparison of ARFE using AOD from AERONET and MODIS

Fig. 8 presents a comparison of the ARFE results using satellite-derived and AERONET AOD. For instance, at SSA 0.925 and SZA 30°–35°, ARFE was –0.64 Wm^{-2} for AERONET and –0.60 Wm^{-2} for MODIS. A larger difference was obtained at SSA 0.875 and SZA 45°–50° where ARFE was –0.43 Wm^{-2} and –0.65 Wm^{-2} for AERONET and MODIS, respectively. However, for most of the ARFE values where we had AOD data from MODIS and AERONET, the results were close to each other with average and maximum differences of 0.073 Wm^{-2} (absolute values) and 0.22 Wm^{-2}, respectively. The ARFE at surface was sometimes overestimated by the satellite data, but in other cases, it was underestimated, not showing any defined tendency or bias. These results give us confidence on the applicability of the methodology presented here to evaluate radiative effects of aerosols in regions where only irradiance measurements and satellite-derived AOD measurements are available.

Going deeper in our analysis, the ARFE at the surface was determined by the difference between the observed and the modeled radiation. The concern about the role of aerosols and their effect on the Earth-atmosphere system requires observations at multiple temporal and spatial scales. MODIS is the main AOD monitoring satellite instrument, and its accuracy and uncertainty need to be routinely validated against ground-based measurements. The comparison between the ARFE obtained from ground-based AOD measurements from AERONET and the ARFE obtained using MODIS measurements confirmed the consistency between them. The inter-comparison between the MODIS AOD and the AERONET AOD measurements shows that MODIS AOD is a suitable alternative to the surface determination of aerosol radiative forcing efficiency, even in the UV-B region.

4. Summary and concluding remarks

In this work, a data set of UV-B measurements in the period 2000–2013, AERONET and improved MODIS AOD data at 340 nm, and

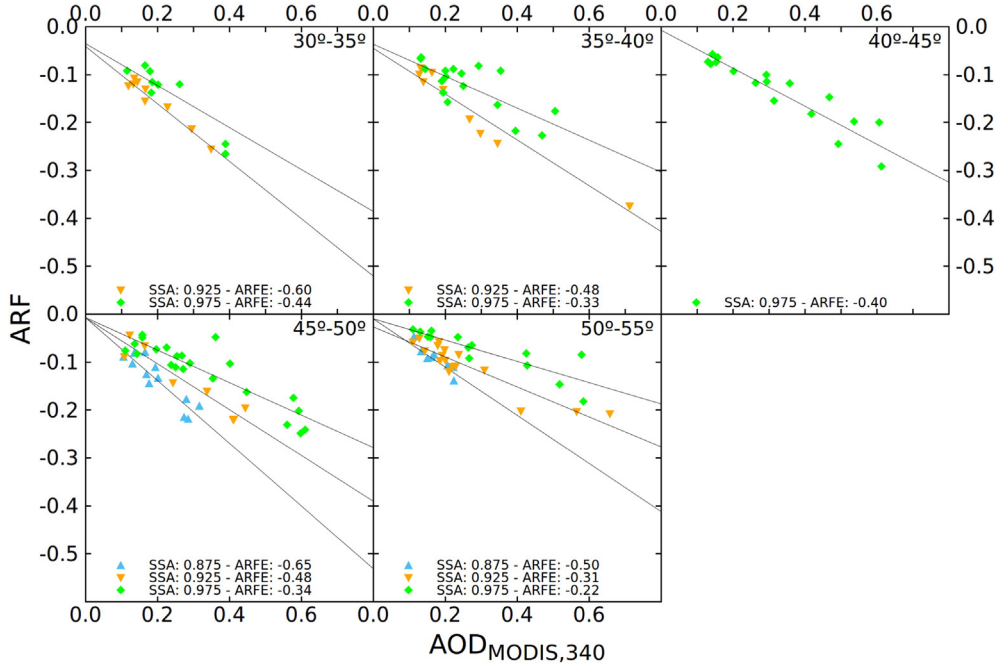

Fig. 6. ARF in the UV-B region as a function of AOD at 340 nm (obtained from MODIS retrievals at 550 nm and Learning Machine Methods). The ARFE for different SZA (5º intervals) and SSA (0.05 unit intervals) are indicated in each panel.

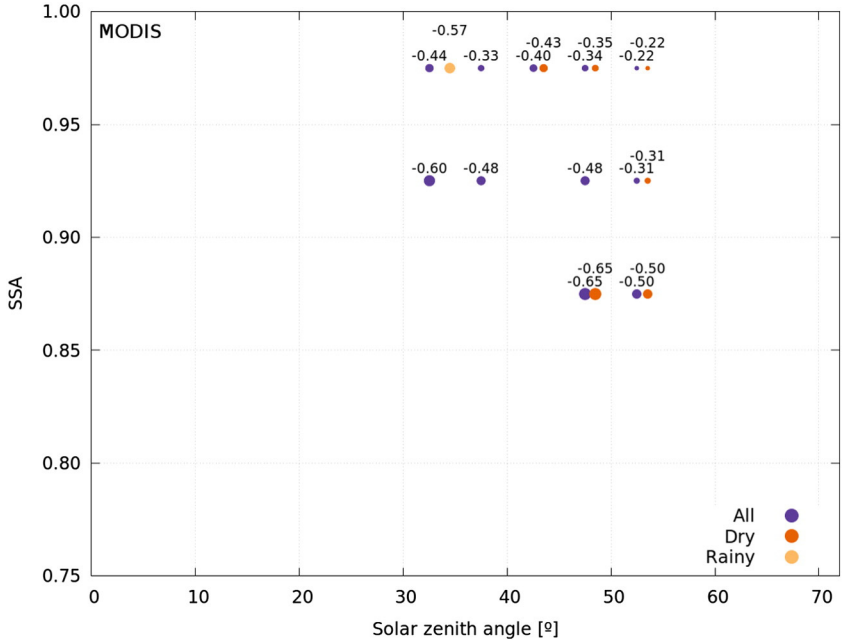

Fig. 7. ARFE in the UV-B region for different SSA and SZA intervals for dry and rainy seasons. AOD values were calculated from MODIS measurements. ARFE values correspond to the slopes shown in Fig. 6. Each set of data (all, dry, and rainy) is plotted at the center of the SSA and SZA intervals.

aerosol-free calculations carried out with the TUV 4.1 radiative transfer model were used to analyze for the first time the effect of the aerosols on the UV-B irradiance through the ARF and ARFE parameters at the surface and under cloudless conditions in Córdoba City.

The long-term data sets of AOD measurements from an AERONET station and from MODIS satellite were analyzed in terms of climatological characterization. The AOD and the g parameter taken from AERONET were used as input for the TUV model in order to determine the instantaneous SSA at 340 nm at the surface under cloud-free conditions. A similar procedure was used by Cordero et al. (2014) in Santiago, finding that the SSA at 350 nm ranged from 0.6 to 0.8. This parameter was used to analyze the effect of the absorptive properties of the aerosols on ARFE ($0.75 \leq SSA \leq 0.99$). The results were also analyzed in terms of the SZA ($10^{\circ} \leq SZA \leq 70^{\circ}$). Here, it was found that ARFE was larger (in absolute value) for absorbing particles (low SSA) and smaller SZA (shorter direct radiation path). The results showed that $ARFE_{UV\text{-}B}$ ranged from -1.76 Wm^{-2} to -0.11 Wm^{-2} with an average value of -0.61 Wm^{-2}. As ARFE depends on the wavelength range of the radiation measurements and on the AOD wavelength of interest a direct comparison among all the ARFE values of the different works (e.g., Lyamani et al., 2006; Dumka and Kaskaoutis, 2014; Chen et al., 2015) is not always possible. When comparing our results with works obtained in the UV range, we found that they are in close agreement with the results for other regions of the world, not only in the absolute

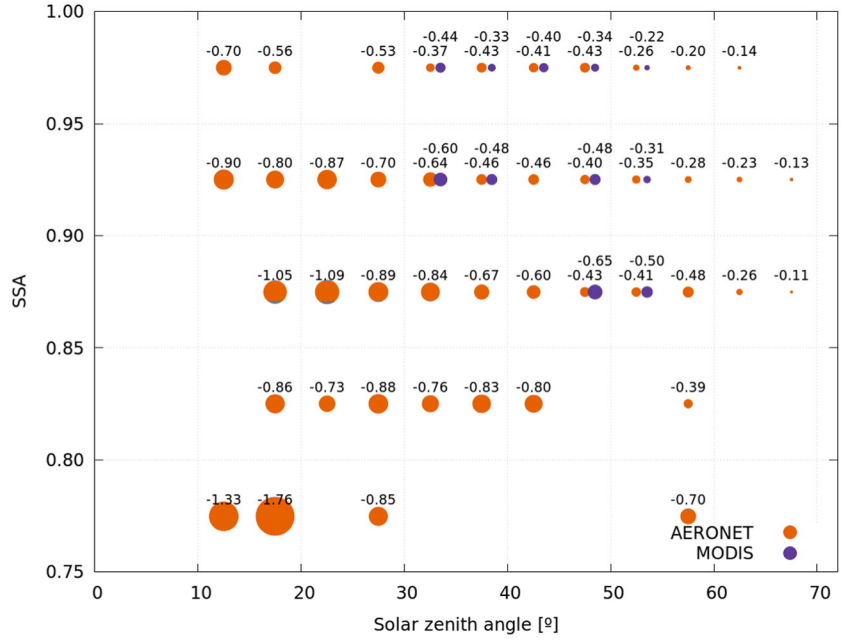

Fig. 8. Comparison between ground-based and satellite-based ARFE in the UV-B region for different SSA and SZA intervals. ARFE values correspond to the slopes shown in Figs. 3 and 6. Each set of data (AERONET and MODIS) is plotted at the center of the SSA and SZA intervals.

values (García et al. (2006), Kazadzis et al. (2009), Meloni et al. (2004), Nikitidou et al. (2013)) but also in the behavior shown respect to the SSA and SZA. Regarding to the ARFE obtained through AOD taken from satellite observations, it was found that $ARFE_{UV\text{-}B}$ ranged from −0.65 Wm^{-2} to −0.22 Wm^{-2} with an average value of –0.43 Wm^{-2}. Analysis of rainy and dry seasons did not show significant differences regarding the ARFE. The comparison of the results showed that, once corrected, satellite AOD retrievals were a suitable option to complement the irradiance measurement in order to calculate the ARFE. In this way, it is possible to evaluate the radiative parameters of the aerosols for other regions of the World where only irradiance measurements are available.

The results of this work highlight the importance of the aerosol type (different SSA) in the quantification of the aerosol radiative forcing and the importance that aerosols have on the Earth radiation budget. This work emphasizes that SSA should be determined with high accuracy in the UV-B due to its relevance in the ARFE determination (Dumka and Kaskaoutis, 2014). In addition, this work reveals that ARFE is mostly governed by AOD and SSA at a given wavelength and in second place by other meteorological variables prevailing in the region.

Acknowledgments

We thank CONICET (PIP 2013–2015 grant number 1120120100004CO), ANPCyT (PICT 2014 grant number 0876), and SeCyT-UNC (grant number 05/C275) for partial support of the work reported here. We thank the AERONET principal investigator Brent Holben for establishing and maintaining the site used in this investigation. We thank the science and support teams of MODIS for their data. Bethania L. Lanzaco and Mariana Achad thank CONICET for graduate and postdoctoral fellowships, respectively.

References

Achad, M., López, M.L., Palancar, G.G., Toselli, B.M., 2013. Retrieving the relative contribution of aerosol types from single particle analysis and radiation measurements and calculations: a comparison of two independent approaches. J. Aerosol Sci. 64, 11–23.

Andrada, G., Palancar, G.G., Toselli, B.M., 2008. Using the optical properties of aerosols from the AERONET database to calculate surface solar UV-B irradiance in Córdoba, Argentina. Comparison with measurements. Atmos. Environ. 42, 6011–6019.

Antón, M., Gil, J.E., Fernández-Gálvez, J., et al., 2011. Evaluation of the aerosol forcing efficiency in the UV erythemal range at Granada, Spain. J. Geophys. Res. 116 (D20), D20214. http://dx.doi.org/10.1029/2011JD016112.

Bush, B.C., Valero, F.P.J., 2003. Surface aerosol radiative forcing at Gosan during the ACE-Asia campaign. J. Geophys. Res. 108 (D23), 8660.

Chen, H., Cheng, T., Gu, X., Wu, Y., 2015. Characterization of aerosols in Beijing during severe aerosol loadings. Atmos. Environ. 119, 273–281.

Cordero, R.R., Seckmeyer, G., et al., 2014. Aerosol effects on the UV irradiance in Santiago de Chile. Atmos. Res. 149, 282–291.

Dichter, B.K., Beaubien, A.F., Beaubien, D., 1993. Development and characterization of a new solar ultraviolet-B irradiance detector. J. Atmos. Ocean. Technol. 10, 337–344.

Dubovik, O., Smirnov, A., Holben, B.N., King, M.D., Kaufman, Y.J., Eck, T.F., Slutsker, I., 2000. Accuracy assessments of aerosol optical properties retrieved from AERONET sun and sky-radiance measurements. J. Geophys. Res. 105, 9791–9806.

Dumka, U.C., Kaskaoutis, D.G., 2014. In-situ measurements of aerosol properties and estimates of radiative forcing efficiency over Gangetic–Himalayan region during the GVAX field campaign. Atmos. Environ. 94, 96–105.

García, O.E., Díaz, A.M., Expósito, F.J., Díaz, J.P., Gröbner, J., Fioletov, V.E., 2006. Cloudless aerosol forcing efficiency in the UV region from AERONET and WOUDC databases. Geophys. Res. Lett. 33 (23), L23803. http://dx.doi.org/10.1029/2006GL026794.

Haywood, J., Boucher, O., 2000. Estimates of the direct and indirect radiative forcing due to trophosferic aerosols : a review. Rev. Geophys. 513–543.

Holben, B.N., Eck, T.F., Slutsker, I., Tanré, D., Buis, J.P., Setzer, A., Vermote, E., Reagan, J.A., Kaufman, Y.J., Nakajima, T., Lavenu, F., Jankowiak, I., Smirnov, A., 1998. AERONET—a federated instrument network and data archive for aerosol characterization. Remote Sens. Environ. 66 (1), 1–16.

IPCC, 2007. Climate change 2007: synthesis report. In: Core Writing Team, Pachauri, R.K., Reisinger, A. (Eds.), Contribution of Working Groups I, II and III to the Fourth Assessment Report of the Intergovernmental Panel on Climate Change. IPCC, Geneva, Switzerland.

Kaufman, Y.J., Tanré, D., Remer, L.A., Vermote, E.F., Chu, A., Holben, B.N., 1997. Operational remote sensing of tropospheric aerosol over land from EOS moderate resolution imaging spectroradiometer. J. Geophys. Res. Atmos. 102 (D14), 17051–17067.

Kazadzis, S., Kouremeti, N., Bais, A., Kazantzidis, A., Meleti, C., 2009. Aerosol forcing efficiency in the UVA region from spectral solar irradiance measurements at an urban environment. Ann. Geophys. 27, 2515–2522. http://dx.doi.org/10.5194/angeo-27-2515-2009.

Lanzaco, B., L.E., Olcese, G.G., Palancar, Toselli, B.M., 2015. A method to improve MODIS AOD values: application to South America. Aerosol Air Qual. Res. http://dx.doi.org/10.4209/aaqr.2015.05.0375.

Levy, R.C., Mattoo, S., Munchak, L.A., Remer, L.A., Sayer, A.M., Patadia, F., Hsu, N.C., 2013. The Collection 6 MODIS aerosol products over land and ocean. J. Atmos. Meas. Tech. 6 (11), 2989–3034.

López, M.L., Palancar, G.G., Toselli, B.M., 2012. Effects of stratocumulus, cumulus, and cirrus clouds on the UV-B diffuse to global ratio: experimental and modeling results. J. Quant. Spectrosc. Radiat. Transf. 113, 461–469.

Lyamani, H., Olmo, F.J., Alcántara, A., Alados-Arboledas, L., 2006. Atmospheric aerosols during the 2003 heat wave in southeastern Spain II: microphysical columnar properties and radiative forcing. Atmos. Environ. 40 (2006), 6465–6476.

Madronich, S., 1987. Photodissociation in the atmosphere: 1. Actinic flux and the effects of ground reflections and clouds. J. Geophys. Res. 92, 9740–9752.

Mckenzie, R.L., Matthews, W.A., Johnston, P.V., 1991. The relationship between erythemal UV and ozone, derived from spectral irradiance measurements. Geophys. Res. Lett. 18, 2269–2272.

Meloni, D., di Sarra, A., Di Iorio, T., Fiocco, G., 2004. Direct radiative forcing of Saharan dust in the Mediterranean from measurements at Lampedusa Island and MISR spaceborne observations. J. Geophys. Res. 109, D08206. http://dx.doi.org/10.1029/2003JD003960.

Neckel, H., Labs, D., 1984. The solar radiation between 3300 and 12500 Å. Sol. Phys. 90, 205–258.

Nikitidou, E., Kazantzidis, a., De Bock, V., H., De Backer, 2013. The aerosol forcing efficiency in the UV region and the estimation of single scattering albedo at a typical West European site. Atmos. Environ. 69, 313–320. http://dx.doi.org/10.1016/j.atmosenv.2012.12.035.

Olcese, L.E., Toselli, B.M., 2002. Some aspects of air pollution in Córdoba, Argentina. Atmos. Environ. 36, 299–306.

Palancar, G.G., 2003. Estudio de procesos cinéticos y radiativos de interés atmosférico Ph.D. Thesis Universidad Nacional de Córdoba, Argentina.

Palancar, G.G., Toselli, B.M., 2002. Erythemal ultraviolet irradiance in Cordoba, Argentina. Atmos. Environ. 36, 287–292.

Palancar, G.G., Toselli, B.M., 2004. Effects of meteorology on the annual and interannual cycle of the UV-B and total radiation in Cordoba City, Argentina. Atmos. Environ. 38, 1073–1082.

Papadimas, C.D., Hatzianastassiou, N., Matsoukas, C., Kanakidou, M., Mihalopoulos, N., Vardavas, I., 2012. The direct effect of aerosols on solar radiation over the broader Mediterranean basin. Atmos. Chem. Phys. 12 (15), 7165–7185. http://dx.doi.org/10.5194/acp-12-7165-2012.

Petrenko, M., Ichoku, C., Leptoukh, G., 2012. Multi-sensor aerosol products sampling system (MAPSS). J. Atmos. Meas. Tech. 5 (5), 913–926.

Ramachandran, S., Srivastava, R., Kedia, S., Rajesh, T.A., 2012. Contribution of natural and anthropogenic aerosols to optical properties and radiative effects over an urban location. Environ. Res. Lett. 7 (3), 034028. http://dx.doi.org/10.1088/1748-9326/7/3/034028.

Remer, L.A., Kleidman, R.G., Levy, R.C., Kaufman, Y.J., Tanré, D., Mattoo, S., ... Holben, B.N., 2008. Global aerosol climatology from the MODIS satellite sensors. J. Geophys. Res. Atmos. 113 (D14), D14S07.

Van Hoosier, M.E., Bartoe, J.D., Brueckner, G.E., Printz, D.K., 1987. Solar Irradiance Measurements 120–400 nm from Space Lab-2. IUGG Assembly, Vancouver.

Vapnik, V., 1995. The Nature of Statistical Learning Theory. Springer-Verlag, New York.

Yu, H., Kaufman, Y.J., Chin, M., et al., 2006. A review of measurement-based assessments of the aerosol direct radiative effect and forcing. Atmos. Chem. Phys. 6 (3), 613–666. http://dx.doi.org/10.5194/acp-6-613-2006.

Zerefos, C.S., 1997. Factors influencing the transmission of solar ultraviolet irradiance through the Earth's atmosphere. In: Zerefos, C.S., Bais, A.F. (Eds.), Solar Ultraviolet Radiation, Modeling, Measurements and Effects, NATO-ASI Series vol. 52. Springer, Verlag, pp. 133–142.